Progress In Electromagnetics Research, PIER 16, 1–33, 1997

POLARIMETRIC DETECTION OF SLOWLY MOVING TARGETS EMBEDDED IN STATIONARY GROUND CLUTTER

X. Morin, E. Pottier, and J. Saillard

I.R.E.S.T.E. Laboratoire S.E.I.
(Systèmes Electroniques et Informatiques)
EP C.N.R.S. 63
La Chantrerie, CP 3003
44087 Nantes Cedex 03, France

C. Pasdeloup and C. Delhote

L.C.T.A.R. (Le Centre THOMSON d'Applications Radar)
6 rue Nieuport, BP 86
78143 Vélizy-Villacoublay Cedex, France

1. Introduction
2. Device and Data
- 2.1 The CIM Radar for Stationary or Slowly Moving Target Detection
- 2.2 Clutter and Target Measurements
- 2.3 Notation

3. Polarimetric Parameters
- 3.1 Definition
- 3.2 Behaviour of the Measured Polarimetric Parameters

4. Detection Algorithms
- 4.1 Introduction
- 4.2 Non-Parametric Methods
- 4.3 Parametric Methods

5. Results for the Non-Parametric Methods
- 5.1 Probabilities of Detection and False Alarm Calculation
- 5.2 Detector Setup

5.3 Results
5.4 Conclusion
6. Results for the Parametric Methods
6.1 Auto-Regressive Methods
6.2 VPA
7. Conclusion
Acknowledgments
References

1. INTRODUCTION

Many radar detection algorithms use both the amplitude and Doppler informations of the backscattered wave or the complex coherent wave measured in only one receiving polarization channel. Usually, detecting moving targets in stationary clutter is carried out by Doppler filtering. This technique is unfitted when targets and clutter are moving at approximately the same speed, as it is in this study, or when the radar Doppler ambiguity is small. This is a limitation of actual radar systems. A new dimension has been added in order to overcome such problem : radar polarimetry.

Radar polarimetry, based on the measurement of the complete radar scattering matrix, allows to define new detection schemes. In this paper, some of these new detection algorithms are applied to real data measurements, and compared, whenever possible, to single channel processing.

Clutter and target measurements have been made possible with CIM, a Ka-band high-resolution polarimetric radar developed by L.C. T.A.R. (Le Centre THOMSON d'Applications Radar) for the detection of targets in slow-moving stationary clutter environments. In the first part of this paper, a short description of this system and the related data are given. Polarimetry gave birth to several new descriptive radar target detection parameters, among them: entropy (H), polarization degree (p), Signal Span (SS), phase difference, ellipticity (τ) and orientation (ϕ). Thus polarimetric parameter behaviour is not identical for clutter and for targets with clutter, and could lead to the improvement of radar detection algorithms. This makes up the second part of this paper. Then, different detection algorithms are presented. They are split in two different categories: the first approach uses a statistical model of clutter and of target-in-clutter. The optimal algorithm and sub-optimal methods are also tested and we have derived theoretically

and evaluated the Maximum Likelihood Ratio for a K law distribution assumption.

The second approach uses a parametric description of the backscattered waves. We propose a new algorithm based on an autoregressive modelling of the polarimetric clutter fluctuations.

Then, the results are presented, often in terms of the probability of detection as a function of the target to clutter power ratio. The probabilities of false alarm (Pfa) that we use may seem unrealistically too high to the readers, but the small number of available data is the reason why it was impossible to work with a lower Pfa.

Finally, as the CIM radar is not a full polarimetric system, it is important to specify that all the detection algorithms that will be presented in this paper do not utilize further distinctive parameters recovered from higher order complete Sinclair [S (2×2)], Kennaugh [K (4×4)], covariance [$\Sigma(3 \times 3)$] matrix formulations or group-theory, Lie aspects as target entropy, OPCE coefficients and "relative co-pol phase difference" or "phase correlation coefficient", etc [4,5,7].

2. DEVICE AND DATA

2.1 The CIM Radar for Stationary or Slowly Moving Target Detection

The CIM radar has been developed by L.C.T.A.R for the detection of slowly moving or stationary vehicles hidden in ground clutter. It is a high-resolution radar, using polarization diversity on reception. The radar CIM is conceptually a non-coherent device. However, coherency is made possible and locally restored by using a stationary fixed trihedral reference target. Its characteristics are summarized in Figure 1.

2.2 Clutter and Target Measurements

The clutter backscatter was measured during the autumn of 1993 at the L.C.T.A.R. outdoor measurements base. Each elementary clutter set is made up, for a given azimuth and a given elevation, of a set of 15 range profiles of 1000 resolution cells each, which corresponds to an acquisition time around 100 ms. For each acquisition, the wind speed and direction are registered with high accuracy. A long time period of measurement is fixed to 10 seconds, which corresponds to an equivalent "antenna rotation" speed of $\pi/5$ rd/s.

	Characteristics
Type of modulation	FM-CW
Carrier frequency	Ka band
Emitted polarization	Circular
Received polarization	Simultaneously two orthogonal polarizations (A and B)
Minimal size of one resolution cell	< 50 cm
Ambiguous speed	± 0,32 m/s
Speed resolution	± 0,04 m/s
Mid-power angle (azimuth)	< 1 degree

Figure 1. CIM radar characteristics.

To illustrate the algorithms presented in this paper, two kinds of clutter have been selected, as can be seen from inspection of Figure 2. The edge of the forest, where a target is present, will be used to illustrate the detection test scenario, and the hedge and house configuration defines the specific test targets as treated in the part of this paper concerning the polarimetric parameters.

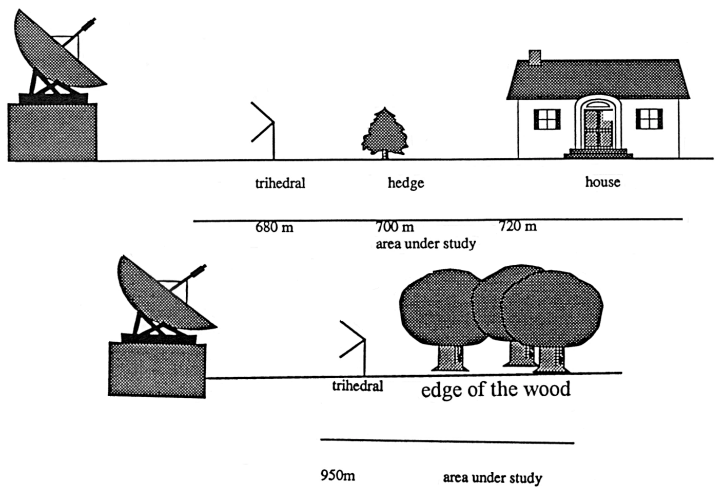

Figure 2. Description of the radar scattering environment.

Targets were first measured at the CELAR (Centre Electronique de l'Armement) outdoor measurements base, using the same CIM radar. Then, the range profiles of the targets are artificially added to the radar scattering environment range profiles, with a given target-to-clutter ratio.

2.3 Notation

The radar return is measured and expressed in a polarimetric Sinclair vector formulation; i.e., back-scatter complex phasor in contrast to forward propagation Jones vector [3] which must strictly be treated separately [6,7,38].

$$\underline{X} = \begin{bmatrix} XA \\ XB \end{bmatrix} = \begin{bmatrix} XA_i + jXA_q \\ XB_i + jXB_q \end{bmatrix} = \begin{bmatrix} |XA|e^{j\delta_A} \\ |XB|e^{j\delta_B} \end{bmatrix} \tag{1}$$

where XA and XB denote A and $B = A_\perp$ part of the received signal, and (i, q) denote the in-phase and quadrature part of each of these components.

We define $\underline{\tilde{X}}$ as the notation which will be used for the centered form of $\underline{X}$

$$\underline{\tilde{X}} = \underline{X} - E[\underline{X}] = \begin{bmatrix} \tilde{X}A \\ \tilde{X}B \end{bmatrix} = \begin{bmatrix} |\tilde{X}A|e^{j\Phi_{\tilde{X}A}} \\ |\tilde{X}B|e^{j\Phi_{\tilde{X}B}} \end{bmatrix} \tag{2}$$

The coherency matrix of the polarimetric Sinclair vector is

$$\Sigma = E\left\{\underline{\tilde{X}}\,\underline{\tilde{X}}^{*T}\right\} = \sigma \begin{bmatrix} 1 & \rho\sqrt{\gamma} \\ \rho^*\sqrt{\gamma} & \gamma \end{bmatrix} \tag{3}$$

with

$$\sigma = E\left\{|\tilde{X}A|^2\right\};\quad \gamma = \frac{E\left\{|\tilde{X}B|^2\right\}}{E\left\{|\tilde{X}A|^2\right\}};\quad \rho\sqrt{\gamma} = \frac{E\left\{\tilde{X}A\tilde{X}B^*\right\}}{E\left\{|\tilde{X}A|^2\right\}}; \tag{4}$$

where σ, γ and ρ represent the different polarimetric co and cross-correlation terms.

3. POLARIMETRIC PARAMETERS

3.1 Definition

Polarimetry produced several new radar detection parameters, including entropy, polarization degree, phase difference, ellipticity and

orientation. The behaviour of these parameters are not identical for clutter and targets-in-clutter. That is why they could lead to improvements in radar detection. This section introduces some of these novel parameters and corresponding results are presented for real data measurements.

The phase difference between Sinclair components is defined as:

$$\delta = \delta_B - \delta_A = \mathrm{Arg}(XB) - \mathrm{Arg}(XA) \tag{5}$$

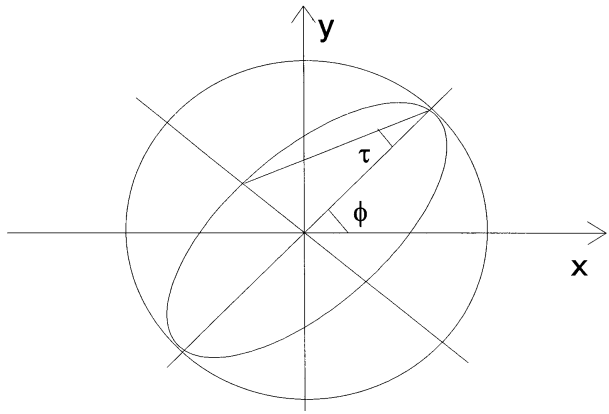

Figure 3. Orientation and tilt angle representation of polarization ellipse.

In the original wave plane, the tip of the electric field trajectory as a function of time is an ellipse. Orientation is the angle between the horizontal axis and the ellipse major axis. This angle, denoted ϕ, restricted to values between $\frac{-\pi}{2}$ and $\frac{\pi}{2}$, can be written as a function of the Sinclair vector [27]

$$tg2\phi = \frac{2|XA||XB|}{|XA|^2 - |XB|^2}\cos\delta \tag{6}$$

The tilt angle τ is the angle measured between the minor and the major axis of the ellipse. τ can take any real value between $\frac{-\pi}{4}$ and $\frac{\pi}{4}$ and can be expressed as

$$\sin 2\tau = \frac{2|XA||XB||}{|XA|^2 + |XB|^2}\sin\delta \tag{7}$$

These two parameters are shown on Figure 3. Results will be focused on the standard deviation of these two angles.

A partially polarized wave can be defined from the expression of the coherency matrix J [26]. This matrix is calculated from the product of the electric field intensity and its conjugate

$$J = \langle \underline{X}\, \underline{X}^{*T} \rangle = \begin{bmatrix} \langle XAXA^* \rangle & \langle XAXB^* \rangle \\ \langle XBXA^* \rangle & \langle XBXB^* \rangle \end{bmatrix} = \begin{bmatrix} J_{11} & J_{12} \\ J_{21} & J_{22} \end{bmatrix} \tag{8}$$

Also, the associated Stokes vector is defined by

$$\underline{g}[\underline{E}] = \begin{bmatrix} g_0 = |XA|^2 + |XB|^2 \\ g_1 = |XA|^2 - |XB|^2 \\ g_2 = 2\mathcal{R}(XAXB^*) \\ g_3 = -2\mathcal{T}(XAXB^*) \end{bmatrix} = g_0 \begin{bmatrix} 1 \\ \cos 2\phi \cos 2\tau \\ \sin 2\phi \cos 2\tau \\ \sin 2\tau \end{bmatrix} \tag{9}$$

It can be shown that the coherency matrix can be written from the Stokes vector [3,6,7,38]

$$J = \frac{1}{2} \begin{bmatrix} g_0 + g_1 & g_2 - jg_3 \\ g_2 + jg_3 & g_0 - g_1 \end{bmatrix} \tag{10}$$

A partially polarized wave can be written as a uncoherent sum of a completely polarized wave and a completely unpolarized wave [5,7]

$$\begin{bmatrix} g_0 \\ g_1 \\ g_2 \\ g_3 \end{bmatrix} = g_0 \begin{bmatrix} 1-p \\ 0 \\ 0 \\ 0 \end{bmatrix} + g_0 \begin{bmatrix} p \\ p\cos 2\phi \cos 2\tau \\ p\sin 2\phi \cos 2\tau \\ p\sin 2\tau \end{bmatrix} \tag{11}$$

The polarization degree (p) is the ratio of the completely polarized wave over the total power of this wave

$$p = \frac{\sqrt{g_1^2 + g_2^2 + g_3^2}}{g_0}, \qquad 0 \le p \le 1 \tag{12}$$

More precisely, p is equal to 1 if the received wave is completely polarized. The determinant of the coherency matrix is then equal to 0. p takes the value 0 if the received wave is completely unpolarized. Then, $J_{11} = J_{22}$ and $J_{12} = J_{21} = 0$. Any intermediate value corresponds to partially polarized waves.

We now introduce another definition of polarimetric entropy (H) introduced by Shane Cloude [8–13] and applied here to a wave instead of a target. The polarimetric entropy (H) of the wave is obtained from the knowledge of the two eigenvalues λ_1 and λ_2 of the coherency matrix J, and is defined as

$$H = -\sum_{k=1}^{2} p_k \log_2(p_k) \tag{13}$$

with

$$p_k = \frac{\lambda_k}{\lambda_1 + \lambda_2} \tag{14}$$

H assumes any real value between 0 and 1. When $H = 0$, the measured environment is so-called perfectly polarized. When $H = 1$, the measured environment is so-called completely unpolarized, and presenting "polarimetric white noise".

3.2 Behaviour of the Measured Polarimetric Parameters

The behaviour of these different polarimetric parameters are given for the specific hedge and house target case, since two motionless objects are naturally present in this scene: the trihedral and the house. These variations correspond to only one set of measurements as has been defined earlier on for the polarimetric phase difference, and 6 consecutive sets of measurements for any other parameter.

The log-scale has been used for polarization degree, polarimetric entropy, ellipticity angle and orientation angle standard deviation, to highlight the differences between clutter and target behaviour, as can be seen on Figure 4.

The phase difference is constant at the trihedral level and random outside this area. The polarization degree is equal to 1 at the trihedral level and very close to 1 at the house level. The hedge does not always have a strong polarization variation (the polarization degree can reach 0.98 at this level). On the other hand, man made targets have the same entropy. They can be easily distinguished from natural clutter. The corresponding entropy gap is close to 25 dB. Obstacles are still clearly set apart from natural clutter when the standard deviations of τ and ϕ are displayed. Still, trihedral and building behaviours are very close to each other. τ is such that 15 dB separates steady targets from the less dispersing clutter spot. This difference reduces to 10 dB when the angle ϕ is considered.

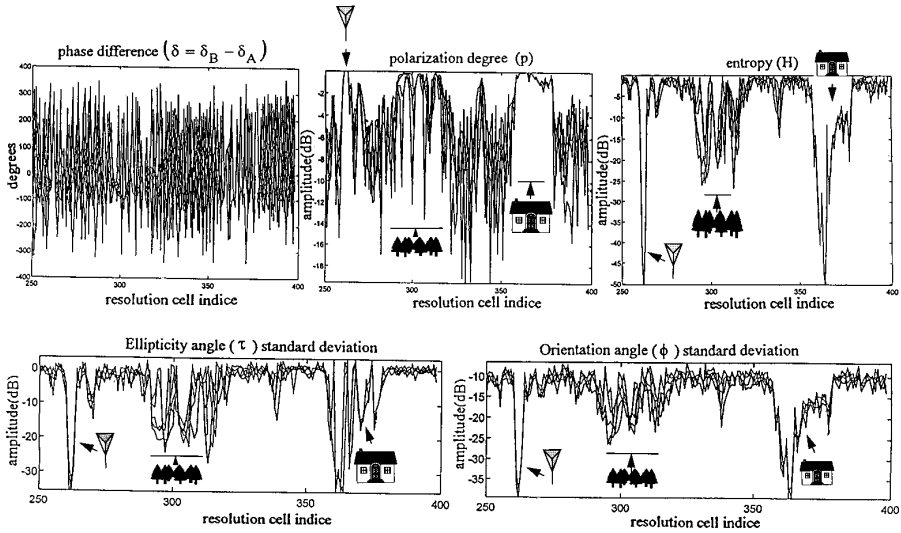

Figure 4. Polarimetric Parameter derivation for 15 consecutive measurements (phase difference) and 6 sets of measurements (other parameters).

We can now conclude that these different polarimetric parameters show important variations when they are studied on natural clutter or man made objects. Using this polarimetric information, we can introduce novel detection procedures and schemes which can be foreseen.

4. DETECTION ALGORITHMS

4.1 Introduction

Two kinds of methods are tested for comparison with the standard detection objective. The first uses the well-known polarimetric likelihood ratio test. Statistical models of clutter and of target-in-clutter are required to compute this algorithm. Here a Gaussian and a non-Gaussian model are selected. Alternative sub-optimal procedures are also tested [29–31].

The second kind of method uses polarimetric and parametric description of the scene. The Poelman Virtual Polarization Algorithm [33–37] and Autoregressive Models [21] are part of this category.

4.2 Non-parametric Methods

The received polarimetric vector $\underline{X}$ enters one of these two categories [1,29]: $\underline{X}$ represents only the clutter (Assumption H_o) or $\underline{X}$ represents both target and clutter (Assumption H_1).

The decision test, the Neyman-Pearson criterion, takes the form of a likelihood ratio:

$$\lambda(\underline{\tilde{X}}) = \frac{P_{H_1}(\underline{\tilde{X}})}{P_{H_o}(\underline{\tilde{X}})} \tag{15}$$

where $P_{H_1}(\underline{\tilde{X}})$ and $P_{H_o}(\underline{\tilde{X}})$ are respectively the conditional probability of $\underline{\tilde{X}}$ in hypothesis H_o and H_1. (15) is then compared to a threshold, T. Two kinds of errors can be made:

- Deciding the absence of a target when it is actually present.
- Deciding the presence of a target when only clutter is present.

This misinterpretation is commonly called probability of false alarm (Pfa) and its value is noted as:

$$\text{Pfa} = P_{H_o}\left\{\lambda(\underline{\tilde{X}}) > T\right\} \tag{16}$$

whereas, the probability of detection (Pd) is given by:

$$\text{Pd} = P_{H_1}\left\{\lambda(\underline{\tilde{X}}) > T\right\} \tag{17}$$

T is an adaptive threshold. It depends on the desired probability of false alarm. The Neyman-Pearson test is optimal in the sense that, for a fixed value of Pfa, it maximizes the probability of detection, Pd.

The most common and most often used Probability Density Function (PDF), is the Gaussian distribution. Here the random variable $\underline{\tilde{X}}$ is assumed to fit a vectorial Gaussian law [14,23,24,29,39].

$$P(\underline{\tilde{X}}) = \frac{1}{\pi^2|\Sigma|}\exp\left(-\underline{\tilde{X}}^{*T}\Sigma^{-1}\underline{\tilde{X}}\right) \tag{18}$$

Taking the neperian logarithm of the Maximum Likelihood Ratio (MLR) leads to the following well known expression

$$\underline{\tilde{X}}^{*T}\left(\Sigma_c^{-1}-\Sigma_{c+t}^{-1}\right)\underline{\tilde{X}}+\ln\frac{|\Sigma_c|}{|\Sigma_{c+t}|} \tag{19}$$

where the subscripts c and $c+t$ respectively stand for clutter and target in clutter. (19) has to be compared to $\ln(T)$. The above relation can be rewritten as a difference of two distances

$$d_c(\underline{\tilde{X}})-d_{c+t}(\underline{\tilde{X}}) \tag{20}$$

which is lower, equal or greater to $\ln(T)$. If we derive the equation (20) versus the polarimetric parameters of the covariance matrix Σ, it has been shown that [29]

$$\begin{aligned} d_i(\underline{\tilde{X}}) = {} & \frac{|\tilde{X}A|^2}{\sigma_i\left(1-|\rho_i|^2\right)}+\frac{|\tilde{X}B|^2}{\sigma_i\gamma_i\left(1-|\rho_i|^2\right)}-\frac{2|\rho_i||\tilde{X}A||\tilde{X}B|}{\sigma_i\sqrt{\gamma_i}\left(1-|\rho_i|^2\right)} \\ & \times\cos(\Phi_{\tilde{X}A}-\Phi_{\tilde{X}B}-\Phi_{\rho_i})+\ln(\gamma_i)+\ln\left(\sigma_i\left(1-|\rho_i|^2\right)\right) \end{aligned} \tag{21}$$

where $i=c$ or $c+t$. This detector is said to be optimal in the sense that it uses the entire polarimetric information: polarimetric amplitude ($\left|\tilde{X}A\right|, \left|\tilde{X}B\right|$) and relative polarimetric phase difference ($\Phi_{\tilde{X}A}-\Phi_{\tilde{X}B}$). The Optimal Polarimetric Detector (OPD) then applies weighting (the weights are combinations of σ_i, γ_i and ρ_i as shown in expression (21)) to the radar measurements before making its decision [29], a concept which was originally developed for the Optimal Polarimetric Matched Filter (OPMF) and introduced by W.M. Boerner as described in [4,5,7].

However, as the range resolution of radar systems improved, the clutter appeared less homogeneous. New descriptions of clutter and targets-in-clutter were found as models [23,24]. The K-PDF stands as a good model for nonhomogeneous scenes. For example, backscattering from meadows, trees, waves on water surfaces, are all random variables well-modelled by the K law. The non-homogeneity is introduced by modelling the PDF of the random variable $\underline{\tilde{X}}$ as the product

of a Gamma distribution, characterizing the spatial variability of intensity g, and a Gaussian distribution representing the speckle, $\underline{\tilde{Y}}$ [2,23,24,29,40,41]:

$$\underline{\tilde{X}} = \sqrt{g}\,\underline{\tilde{Y}} \tag{22}$$

with

$$P(g) = \frac{1}{\bar{g}} \left(\frac{g}{\bar{g}}\right)^{v-1} \frac{1}{\Gamma(v)} \exp\left(-\frac{g}{\bar{g}}\right) \tag{23}$$

in which $\bar{g}$ and v are related to the mean and variance of $P(g)$ as

$$E(G) = \bar{g}v \qquad \text{and} \qquad E(g^2) = \bar{g}^2 v(v+1) \tag{24}$$

Setting $\bar{g} = \frac{1}{\alpha}$ and $v = \alpha$, the one-parameter K-PDF is obtained

$$P(\underline{\tilde{X}}) = \frac{2}{\pi^2 |\Sigma|} \frac{\alpha^{\frac{2+\alpha}{2}}}{\left(\underline{\tilde{X}}^{*T} \Sigma^{-1} \underline{\tilde{X}}\right)^{\frac{2-\alpha}{2}} \Gamma(\alpha)} K_{\alpha-2}\left(\sqrt{2\alpha}\left(\underline{\tilde{X}}^{*T} \Sigma^{-1} \underline{\tilde{X}}\right)^{\frac{1}{2}}\right) \tag{25}$$

where K is the modified Bessel function of second kind and of order v

$$K_v(z) = \frac{1}{2\pi} \frac{I_{-v}(z) - I_v(z)}{\sin(\pi v)} \tag{26}$$

where

$$I_v(z) = \exp(-\frac{1}{2} v\pi j) J_v\left(z e^{j\frac{\pi}{2}}\right) \tag{27}$$

The parameter α is calculated from the higher moments of the signal intensity [2,41]

$$I^{(m)} = \frac{\frac{\left\langle \left|\underline{\tilde{X}} A\right|^{2m} \right\rangle}{\left\langle \left|\underline{\tilde{X}} A\right|^{2} \right\rangle^{m}} + \frac{\left\langle \left|\underline{\tilde{X}} B\right|^{2m} \right\rangle}{\left\langle \left|\underline{\tilde{X}} B\right|^{2} \right\rangle^{m}}}{2} \tag{28}$$

m is the order of the normalized intensity moments. These moments are found to be equal to

$$I^{(m)} = \frac{m!\Gamma(m+\alpha)}{\alpha^m \Gamma(\alpha)} \tag{29}$$

We have shown that taking the logarithm of the MLR leads to the following expression

$$\ln\left(\frac{\bar{g}_c v_c \Gamma(v_c)|\Sigma_c|\left[\bar{g}_c \underline{\tilde{X}}^{*T}\Sigma_c^{-1}\underline{\tilde{X}}\right]^{\frac{2-v_c}{2}} K_{v_{c+t}-2}\left(2\sqrt{\frac{\underline{\tilde{X}}^{*T}\Sigma_{c+t}^{-1}\underline{\tilde{X}}}{\bar{g}_{c+t}}}\right)}{\bar{g}_{c+t} v_{c+t}\Gamma(v_{c+t})|\Sigma_{c+t}|\left[\bar{g}_{c+t}\underline{\tilde{X}}^{*T}\Sigma_{c+t}^{-1}\underline{\tilde{X}}\right]^{\frac{2-v_{c+t}}{2}} K_{v_c-2}\left(2\sqrt{\frac{\underline{\tilde{X}}^{*T}\Sigma_c^{-1}\underline{\tilde{X}}}{\bar{g}_c}}\right)}\right) \tag{30}$$

Then, a comparison between (30) and $\ln(T)$ has to be made. As has been done for the Gaussian case, the expression given in (30) can be rewritten as a difference between two distances

$$d_c(\underline{\tilde{X}}) - d_{c+t}(\underline{\tilde{X}}) \tag{31}$$

If we derive the equation (31) versus the polarimetric parameters of the covariance matrix Σ, we show that

$$\begin{aligned} d_i(\underline{\tilde{X}}) = {} & v_i \ln(\Gamma(v_i)) + \ln(|\Sigma_i|) - \ln\left(K_{v_i-2}\left(2\frac{q_i}{\sqrt{\bar{g}i}}\right)\right) \\ & + \left(\frac{2-v_i}{2}\right)\left(\ln(\bar{g}_i) + 2\ln(q_i)\right);\ i = c, c+t \end{aligned} \tag{32}$$

and

$$q_i^2 = \underline{\tilde{X}}^{*T}\Sigma_i^{-1}\underline{\tilde{X}} \tag{33}$$

The two methods previously discussed are optimal when the different assumptions are encountered. However, there exist sub-optimal methods as the Polarimetric Whitening Filter (PWF) and the Polarimetric Signal Span (PSS).

The Polarimetric Whitening Filter is a simple quadratic algorithm. The principle of this method is investigating the more appropriate channel combination, in order to minimize the coefficient of variation $C_z = \frac{\sigma_z}{m_z}$, where m_z and σ_z are respectively the expectation and the standard deviation of $z = \underline{\tilde{X}}^{*T} A \underline{\tilde{X}}$. A is the unknown, and is assumed to be hermitian positive definite. Provided that the clutter is multi-gaussian distributed and that texture is channel invariant, the

solution is shown to be : $A = \Sigma_x^{-1}$ where Σ_x is the covariance matrix of $\underline{X}$ [29]

$$\underline{\tilde{X}}^{*T} \Sigma_c^{-1} \underline{\tilde{X}} \tag{34}$$

is then compared to a threshold, T. The PWF is not optimal since it ignores the target-plus-clutter covariance information. No appropriate PDF modelling is required. Only the clutter covariance has to be learned.

The Polarimetric Signal Span (PSS) calculates the summation of the intensities measured in each polarization channel [29]

$$\underline{\tilde{X}}^{*T} \underline{\tilde{X}} = \left| \tilde{X} A \right|^2 + \left| \tilde{X} B \right|^2 \tag{35}$$

A comparison is then made between (35) and a threshold, T. This detector does not take into account the phase components of the Sinclair vectors.

4.3 Parametric Methods

The first parametric method presented is the Virtual Polarization Adaptation (VPA), which has been developed by A.J Poelman [33–37], and is based on the assumption that clutter and target-plus-clutter backscattered signals have different polarization states.

The Figure 5 shows the Poelman VPA filter:

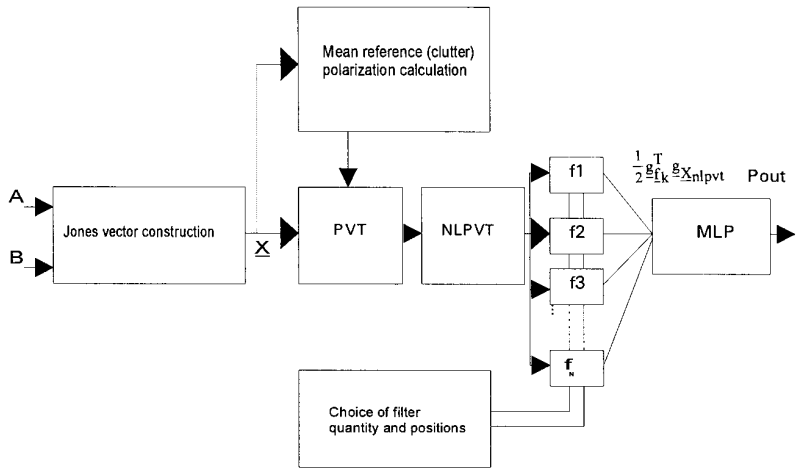

Figure 5. The A. J. Poelman VPA filter setup.

For more details concerning the Poelman VPA processing, the reader is invited to read the originator's papers [33–37] given in references.

The filter response is minimal for clutter echoes. That is due to the values of the coefficients of the set of filters f extracted from the clutter backscatter, the center of which is orthogonal to clutter polarization. Due to polarization differences, orthogonality is lost when a target appears. Output power then increases at the Poelman VPA filter output.

For each resolution cell, the first step of the process calculates the mean temporal Stokes vector

$$\underline{g_m} = \left\langle \underline{g_x} \right\rangle = \begin{bmatrix} g_o \\ g_o \cos 2\phi_m \cos 2\tau_m \\ g_o \sin 2\phi_m \cos 2\tau_m \\ g_o \sin 2\tau_m \end{bmatrix} \tag{36}$$

While operating the Poelman Polarization Vector Translation (PVT) [34], the "cloud" formed by the clutter backscattered Sinclair vectors is recentered on an arbitrary chosen polarization. For this application, the left-hand circular polarization has been chosen because of its closeness to the mean polarization state of the clutter received signals. Using the Huynen Sinclair vector decomposition [15–20], the translated received signal $\underline{X_T}$ can be written

$$\underline{X_T} = \frac{1}{\sqrt{2}} \begin{bmatrix} 1 & j \\ j & 1 \end{bmatrix} \begin{bmatrix} \cos\tau_m & -j\sin\tau_m \\ -j\sin\tau_m & \cos\tau_m \end{bmatrix} \begin{bmatrix} \cos\phi_m & \sin\phi_m \\ -\sin\phi_m & \cos\phi_m \end{bmatrix} \underline{X} \tag{37}$$

The Huynen reference matrix, given in (37), is stored and further multiplied to every Sinclair vector from the next set of measurements.

The non-linear translation filter reduces clutter spread in the polarization space. Thus, weak differences between clutter and targets are increased and revealed. An area of clutter presence is defined around the left-hand circular polarization. Processing the Poelman Non-Linear Polarization Vector Translation (NLPVT) [35] implies that each polarization vector located inside this area comes closer to left-hand circular polarization (North pole of the Poincaré sphere). On the other hand, vectors located outside this area are rejected and transposed towards the orthogonal polarization, i.e. right-hand circular polarization (South pole of the Poincaré sphere) as we can see on Figure 6.

The Poelman Multinotch Logic Product Polarization Filter (MLP) [36, 37] is a reject-band filter in the polarization space. It is

made of a set of simple reject filters which mean polarization is right-hand circular. The filters are placed on concentric rings around the right-hand circular polarization (South pole of the Poincaré sphere).

The output power is calculated as a function of the received and translated signal Stokes vector $\underline{g}_{\underline{X}_{nlpvt}}$ outputted by the Poelman NLPVT filter and the k^{th} notch filter Stokes vector $\underline{g}_{\underline{f}_k}$ (k has a value between 1 and the number of notches, N)

$$P_{out} = 10 \sum_{k=1}^{N} \log_{10} \left(\frac{1}{2} \underline{g}_{\underline{f}_k}^T \underline{g}_{\underline{X}_{nlpvt}} \right) \tag{38}$$

The Figures 6 and 7 show the polarization states of the backscattered wave for a given resolution cell, and the position of the filter notches on the Poincaré planisphere, i.e., the Aitoff-Hammer equal area projection of the spherical surface [3,6,7,38].

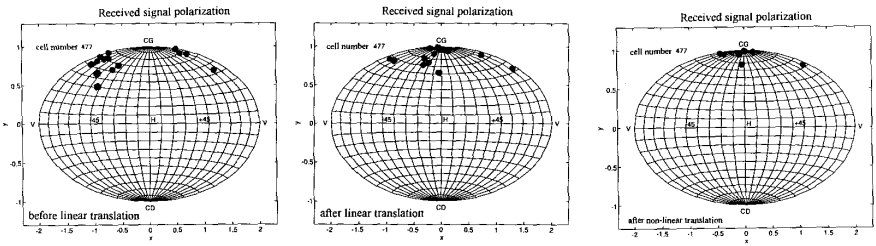

Figure 6. Clutter representation on Aitoff-Hammer equal area projection of Poincaré sphere: before linear translation (left), after linear translation (middle) and after non-linear translation (right).

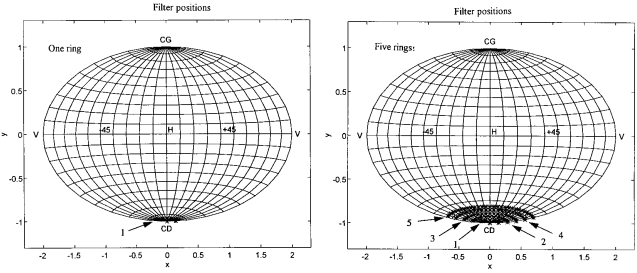

Figure 7. Filter position for only one ring (left) and five rings (right) on Aitoff-Hammer equal area projection of Poincaré sphere.

A second parametric method which is based on the signal autoregressive (AR) analysis can give also a high degree of auto-adaptation. It concerns clutter filtering, which is more selective than the classical techniques of Doppler detection and estimation. The algorithm under study whitens the clutter spectrum, thus achieving an adaptation to the signal backscattered by the target. The different steps of this algorithm are given below.

The algorithm introduced in this paragraph is a prediction scheme. Prior to any processing, several antenna rotations are needed to learn and analyze the background environment. No target is assumed to be present during this training stage, from which a set of coefficients is calculated. After the training stage, these factors are used to predict the expected received signal corresponding to the next antenna rotation. If this prediction is correct, the difference between this signal and its forecast, called the innovation, is a realization of a white Gaussian noise. In each resolution cell, a Fourier Transform of the innovation autocorrelation function is then applied. If the measured spot has not changed, the Power Spectral Density (PSD) energy is equitably shared in all the Doppler filters. If a target appears, the energy is no longer equitably distributed. Energy peaks appear at frequencies proportional to the target speed.

The parameters of the autoregressive analysis are calculated for some range cells where only clutter is present. These cells represent the reference of only noise for the AR clutter modelling. Then, the time predicted polarimetric signal vector $\underline{\hat{X}}(n)$ in a resolution cell is evaluated from the p preceding measures in the same range cell. A classical innovation vector calculation $\underline{\tilde{X}}(n) = \underline{X}(n) - \underline{\hat{X}}(n)$ achieves the clutter spectrum whitening.

A quadratic detection in each Doppler filter, with a range CFAR (Constant False Alarm Rate) is then applied to the innovation process.

Usually, AR procedures use only a one channel receiver. The use of a polarimetric radar gives the opportunity to make a two-dimensional AR signal model, which takes into account both A and $B = A_{\perp}$ polarimetric channels, where A and $B = A_{\perp}$ denote the pair of orthogonal linear polarization states which are used in this study.

The AR method used is the covariance method. The auto-regressive parameters are calculated by minimizing the prediction error power [21]. Three AR algorithms have been compared: the classical non-polarimetric one-channel AR model, the polarimetric one-channel

AR model and the polarimetric two-channel AR model.

For both the one-channel AR model and the polarimetric one channel AR model, the auto-regressive parameters $a(i)$ are calculated by minimizing the estimated prediction error power signal $\hat{\rho}$

$$\hat{\rho} = \frac{1}{N-p} \sum_{n=p}^{N-1} \left| x(n) - \sum_{k=1}^{p} a(k)x(n-k) \right|^2 \tag{39}$$

where $x(n)$ is the signal observed at the output of the channel A or $B = A_\perp$, at time n and is one of the components of the polarimetric signal vector $\underline{X}(n)$, p is the order of the autoregressive model, and N is the number of samples. The index n of $x(n)$ is included in the range $[0, N-1]$. $\hat{\rho}$ is minimized by applying the complex gradient method. The result is

$$\begin{bmatrix} \hat{a}(1) \\ \hat{a}(2) \\ \vdots \\ \hat{a}(p) \end{bmatrix} = \begin{bmatrix} c_{xx}(1,1) & c_{xx}(1,2) & \dots & c_{xx}(1,p) \\ c_{xx}(2,1) & c_{xx}(2,2) & \dots & c_{xx}(2,p) \\ \vdots & \vdots & \dots & \vdots \\ c_{xx}(p,1) & c_{xx}(p,2) & \dots & c_{xx}(p,p) \end{bmatrix}^{-1} \begin{bmatrix} c_{xx}(1,0) \\ c_{xx}(2,0) \\ \vdots \\ c_{xx}(p,0) \end{bmatrix} \tag{40}$$

with

$$c_{xx}(r,k) = \frac{1}{N-p} \sum_{n=p}^{N-1} x^*(n-r)x(n-k) \tag{41}$$

For each channel (A or $B = A_\perp$), the predicted value is given by

$$\hat{x}(n) = \hat{a}(1)x(n-1) + \cdots + \hat{a}(p)x(n-p) \tag{42}$$

Detection is estimated from the knowledge of the Power Spectral Density (PSD) function defined in each resolution cell, either PSD $\{|\tilde{x}_j(n)|\}$ for a one-channel AR with $j = A$ or $j = B = A_\perp$, or PSD $\{|\tilde{x}_A(n)|\} + \text{PSD}\,\{|\tilde{x}_{B=A_\perp}(n)|\}$ for a polarimetric one-channel AR.

Concerning the two-channel polarimetric AR model, the polarimetric signal can be modelled as a complex two-channel signal $\underline{X}(n)$ which is defined by

$$\underline{X}(n) = \begin{bmatrix} x_A(n) \\ x_B(n) \end{bmatrix} \tag{43}$$

where A and $B = A_\perp$ represent the two orthogonal polarimetric channels. The parameters of the autoregressive analysis are estimated

in this case by minimizing the sum of the estimated prediction error powers of the individual channels, for which

$$\hat{\rho} = \text{trace } (\hat{\Sigma}) \tag{44}$$

is minimized with

$$\hat{\Sigma} = \frac{1}{N} \sum_{n} (\underline{X}(n) - \underline{\hat{X}}(n))^* (\underline{X}(n) - \underline{\hat{X}}(n))^T \tag{45}$$

The expressions for the predicted vectors $\underline{\hat{X}}(n)$ are

$$\underline{\hat{X}}(n) = \sum_{r=1}^{p} \Lambda(r) \underline{X}(n-r) \quad \text{with} \quad \dim \Lambda(r) = 2 \times 2. \tag{46}$$

with

$$\hat{\mu} = \text{trace} \left\{ \frac{1}{N} \sum_{n} \left(\sum_{r=0}^{p} \Lambda(r) \underline{X}(n-r) \right)^* \left(\sum_{r=0}^{p} \Lambda(r) \underline{X}(n-r) \right)^T \right\} \tag{47}$$

By minimizing $\hat{\mu}$, we obtain

$$\sum_{k=1}^{p} C_{xx}(r,k) \hat{\Lambda}^T(k) = C_{xx}(r,0) \quad 1 \leq r \leq p \tag{48}$$

hence

$$\begin{bmatrix} \hat{\Lambda}^T(1) \\ \vdots \\ \hat{\Lambda}^T(p) \end{bmatrix} = \begin{bmatrix} C_{xx}(1,1) & \dots & C_{xx}(1,p) \\ \vdots & \vdots & \vdots \\ C_{xx}(p,1) & \dots & C_{xx}(p,p) \end{bmatrix}^{-1} \begin{bmatrix} C_{xx}(1,0) \\ \vdots \\ C_{xx}(p,0) \end{bmatrix} \tag{49}$$

with

$$C_{xx}(r,k) = \frac{1}{N} \sum_{n} \underline{X}^*(n-r) \underline{X}^T(n-k) \tag{50}$$

and

$$\hat{\Sigma} = C_{xx}(0,0) + \sum_{k=1}^{p} C_{xx}(0,k) \hat{\Lambda}^T(k) \tag{51}$$

Detection is estimated from

$$\mathrm{PSD}\left\{|\tilde{x}_A(n)|\right\} + \mathrm{PSD}\left\{|\tilde{x}_{B=A_\perp}(n)|\right\} \tag{52}$$

5. RESULTS FOR THE NON-PARAMETRIC METHODS

5.1 Probabilities of Detection and False Alarm Calculation

Due to the small number of available measurements, the probability of false alarm Pfa has been fixed at a constant high value (6.6×10^{-2}). The detection threshold is then calculated for the first set of measurements, for which no target is present. This threshold is adaptive since it depends upon the resolution cell under consideration. Then, the probability of detection Pd is assessed by counting over-threshold test results in the area where the target is present.

5.2 Detector Setup

For the Whitening filter and Maximum Likelihood tests, the detector comprises two equal size range gates, and a range area (called "security ring") where no data is processed. The first gate is assumed to contain only clutter, while in the second a target is assumed to be present. The security ring is used because the target is not considered as a point target but as a spread one.

Thus, the set of data comprised in the first range gate is assumed to confirm assumption H_o, while data belonging to the second gate are supposed to verify assumption H_1.

A test calculation is made for each Sinclair vector of the central range cell of the second range gate, as can be seen on Figure 8.

This detector is then entirely moved by one resolution range cell. If the assumptions (H_o and H_1 respectively in the first and the second gate) are not satisfied, there is no detection. It happens when both range gates contain only clutter, as during the learning phase (first antenna rotation), when the thresholds were calculated.

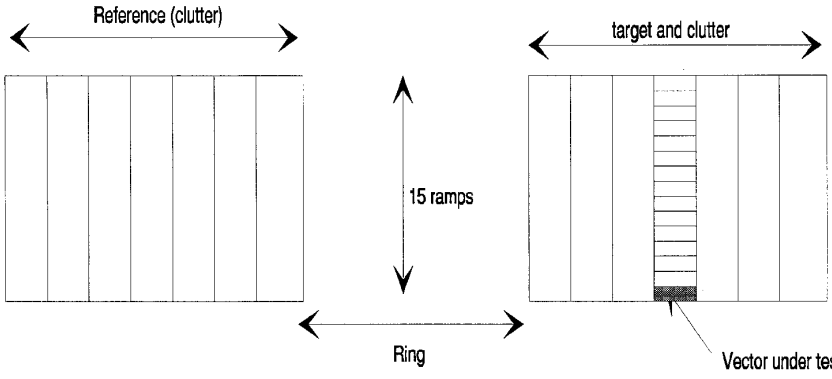

Figure 8. The detector setup. Ring and window sizes are adjustable.

The following curves, on Figure 9, represent the Probability of detection (Pd) as a function of the range gate size. Different curves are shown, each corresponding to a given ring size. The sliding range gate size is successively set to 1,3,5, and 7 resolution cells.

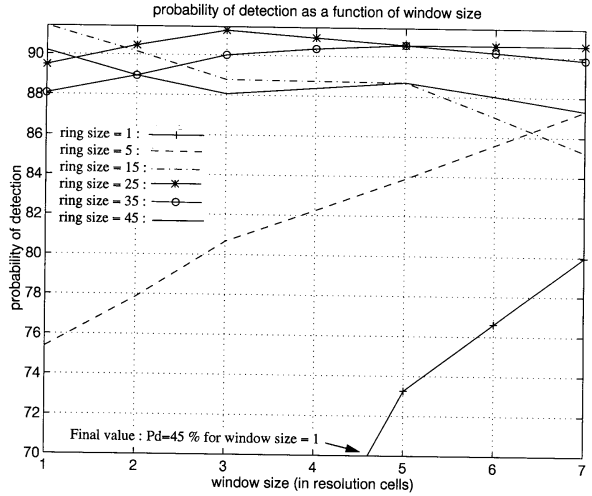

Figure 9. Probability of detection as a function of window size.

It appears that for a given range gate size, the probability of detection increases while the security ring size increases. More precisely, it seems that the choice of a security ring larger than the target is necessary. In addition, the probability of detection is improved when range gate sizes are increased, particularly if the ring size is small. If not, the curve slope can be negative. This is due to false alarms induced by two different kinds of remote clutters. Later on, results will be given for range gates and security ring sizes respectively equal to 7 and 45 resolution cells.

5.3 Results

In this paragraph, the radial target speed is equal to 0.14 m/s. Probabilities of detection (in %) are given as a function of the target-to-clutter ratio (in dB). One and two channel detection schemes are shown on the same graph on Figures 10 and 11.

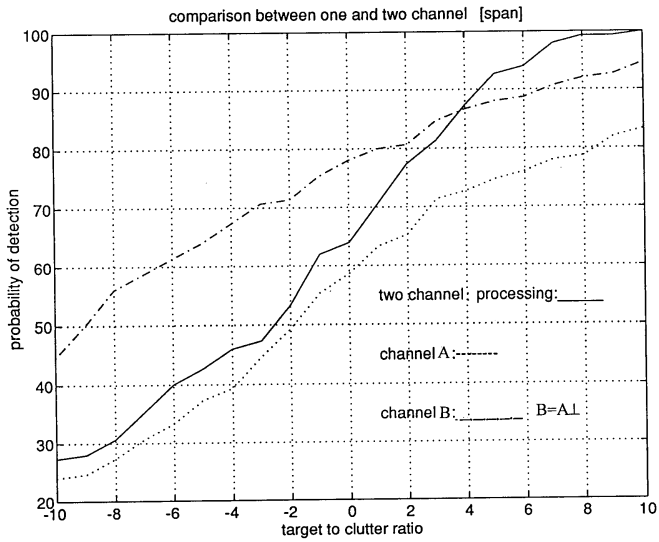

Figure 10. The Signal SPAN detector results.

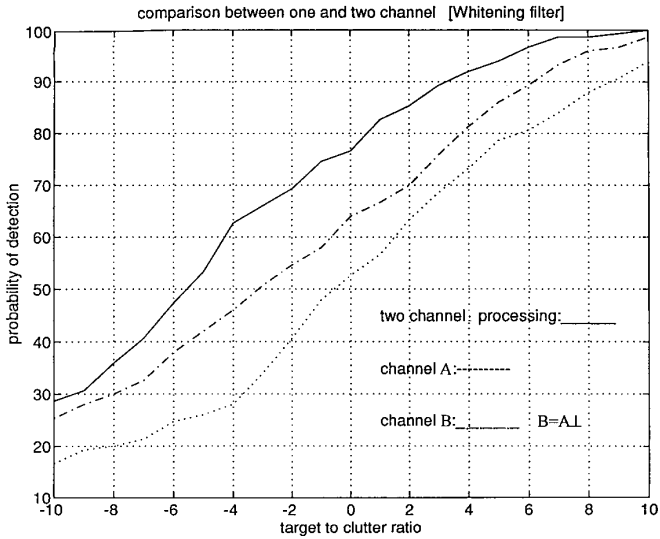

Figure 11. The Whitening Filter results.

Taking the two polarimetric channels into account improves the detection process when the target-to-clutter ratio is greater than 4 dB. From the measurements, we can see that a probability of detection equal to 90% requires a target-to-clutter ratio of 4.5 dB when two polarimetric channels are considered, 6.5 dB if only the channel $B = A_{\perp}$ is read.

Taking two polarimetric channels into account simultaneously results in a large improvement in the Whitening Filter performances. This improvement is equal to about 3 dB compared to the most effective channel (i.e the channel $B = A_{\perp}$). For a probability of detection equal to 90%, a target-to-clutter ratio equal to 3.2 dB is required in the two-channel configuration, 6 dB if only the channel $B = A_{\perp}$ is considered, and 8.6 dB when it is the channel A .

It is known that the Maximum Likelihood Ratio (MLR) tests are optimal. They give better results than those obtained using the preceding methods. The results shown in this section correspond to the edge of the wooded region. Using probability adequation test on the data, the selected clutter appears to be independently K distributed in each channel. The Gaussian PDF, which is a particular case of the K distribution ($\alpha \to \infty$) does not fit the clutter as well. How-

ever, when a two-channel processing is considered, it happens that the Gaussian distributed clutter assumption leads to better results than the K distributed one. This trend is reversed when only one channel is considered. The reason of this reversal is that relation (28) is not optimal for the derivation of α in the two-channel case. (28) is true only if it is assumed that α gets the same value in channel A and channel $B = A_\perp$. The physical meaning of this statement is that the texture is polarization independent. Deriving α more appropriately could be the subject of a future study.

A probability of detection equal to 90% when the K law is selected corresponds to a target-to-clutter ratio of -0.6 dB when A and $B = A_\perp$ channels are both selected. This ratio reaches 1.7 dB and 4.4 dB when only $B = A_\perp$ or A polarization channels respectively are chosen. For the same probability of detection, a signal-to-clutter ratio of -1.2 dB is sufficient when the Gaussian law is considered. Ratios of 5.5 dB are then gained compared to a one-channel device system, since 4.1 dB and 6.8 dB are respectively the measured requested ratios on each of the two channels separately taken.

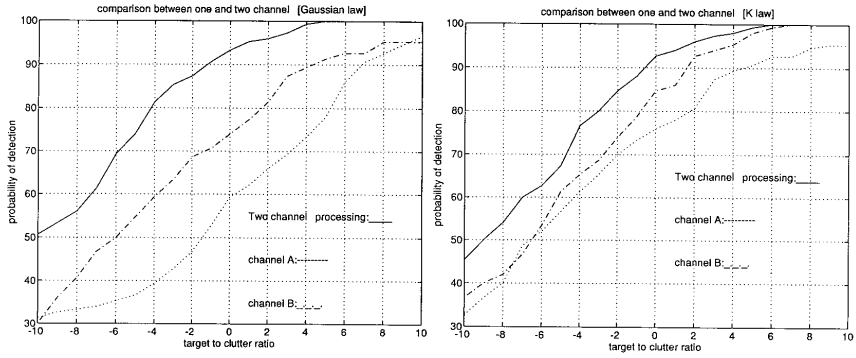

Figure 12. Maximum Likelihood Ratio (MLR) results.

When the two channels are considered, it can be seen that the best method is the Maximum Likelihood Ratio test, for which 3 dB are gained compared to the Whitening Filter results. This last algorithm produces nearly a 2 dB gain compared to the less effective method, the complete polarimetric Signal Span magnitude only, as should be expected since valuable polarimetric phase information was discarded.

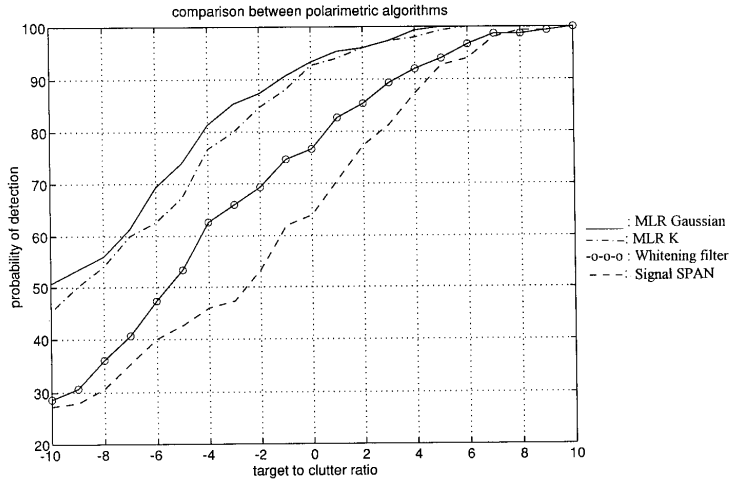

Figure 13. Comparison of Polarimetric Procedures.

5.4 Conclusion

The results show that a reasonable large range gate size combined with a security ring of dimensions at least equal to the target size gives the best results for detection purposes.

The best detection methods are MLR tests and the Whitening Filter. Lastly, the Signal Span method is the least effective polarimetric detector in that critical polarimetric phase differences are not being incorporated into the algorithm.

Taking two orthogonal channels into account significantly improves detector performances compared to a one-channel processing (between 2 dB and 7 dB according to which detector is used, for a given probability of detection : 0.9).

6. RESULTS FOR THE PARAMETRIC METHODS

5.1 Auto-Regressive Methods

For the AR algorithm, a threshold is determined to achieve a probability of false alarm equal to 5×10^{-2}. This threshold is estimated with only one clutter file. A target is then artificially added to the

clutter. The probability of detection is estimated for the most representative target scatterer. To obtain sufficient data for the calculation of the Pd, different positions of the target in the 6 clutter files are considered (there is a 10 second time separation between 2 files). The probability of detection is drawn as a function of the signal-to-clutter ratio for one pulse in the polarization channel A. The AR order p is equal to 2. The two following curves, on Figures 14 and 15, represent the power spectral densities (PSD) before and after the AR treatment for one burst of pulses. The clutter spectrum whitening can then be observed. The detection is realized in each Doppler filter (passing from one Doppler filter to the other corresponds to a radial velocity shift of 0.04 m/s).

A Doppler analysis, applied on the PSD of the innovation signal, provides the visibility factor information, fixed for a Pd of 0.9 and a Pfa equal to 5×10^{-2}. The visibility factor is the minimal signal-to-clutter ratio required to obtain a probability of detection with a fixed probability of false alarm. It is given for one pulse, and the detection is made after a coherent integration of 13 pulses which results in a gain of 11 dB on the signal-to-clutter ratio.

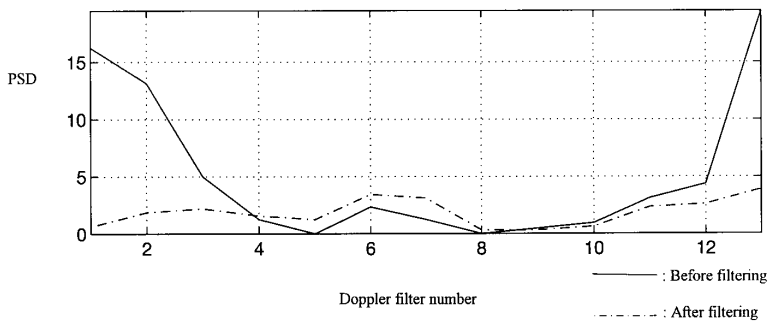

Figure 14. Power Spectral Density/One channel AR/Channel A (only clutter).

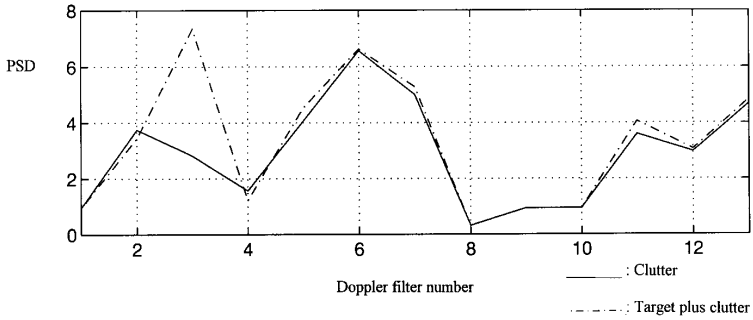

Figure 15. Power Spectral Density/Two channel AR (after filtering). The target to clutter ratio is equal to -7 dB/pulse and the radial velocity is equal to 0.09 m/s.

For these Doppler velocities, the polarimetric one-channel and the polarimetric two-channel algorithms give comparable results. With a two-channel polarimetric radar, the gain obtained for these types of target and clutter is about 2 dB greater than those obtained using only a one channel non-polarimetric radar.

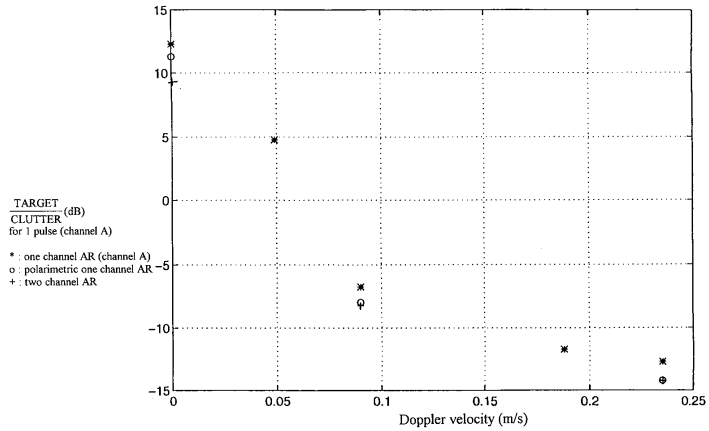

Figure 16. Visibility factor, given for the three algorithms (Pfa=0.05 and Pd=0.9).

6.2 VPA

Results are shown for a single ring of notches. When this method is not applied in a selective manner, results are slightly faint. The reason is that for weak power scatterers, reference polarization variations are very strong. The output power is then minimized, but high. Such a background environment is not likely to serve well for a detection scheme, since it is much too scattered. A solution has been found to solve this problem. Entropy, as presented in the third paragraph, is an indicator of the degree of disorder of a cell, as a function of time. The closer to zero entropy is, the more localized is the cloud of vectors on the Poincaré sphere.

The first step of the process is the calculation of the entropy. Only the resolution cells for which entropy is inferior to an arbitrary chosen threshold (0.5 for this application) are selected. Then, the VPA procedure is applied.

To obtain a probability of detection equal to 0.9, the target-to-clutter ratio must be equal to 2 dB, thus 1.2 dB less compared to the result obtained by using the two-channel Whitening filter. It has to be noted that these results have been obtained only for cells where the clutter is considered as stationary (entropy < 0.5). Furthermore, in the case where a target is located in a very high entropy clutter area, the VPA procedure would be impossible to use in its current state, since it would not lead to good results.

7. CONCLUSION

This paper is about the detection of slowly moving targets embedded in stationary ground clutter. Different detection schemes have been considered and compared with one another. The possible contribution of polarimetry to detection has been figured out.

Some polarimetric parameters have been presented. These variables take different values when they are calculated on clutter and on targets in clutter. Using these parameters to improve detection procedures can be foreseen.

Then, different polarimetric detection schemes have been presented and applied to real data measurements. Whenever possible, the obtained performances have been compared to only-one channel detection results. Well-known detectors have been used: Signal Span, Whitening Filter, Gaussian modelized Maximum Likelihood Ratio and the

A.J. Poelman Vector Polarization Adaptation. We have developed a new derivation of the Neyman-Pearson test for a K-law distribution assumption. Also, we have proposed a new detection algorithm based on auto-regressive clutter modelling.

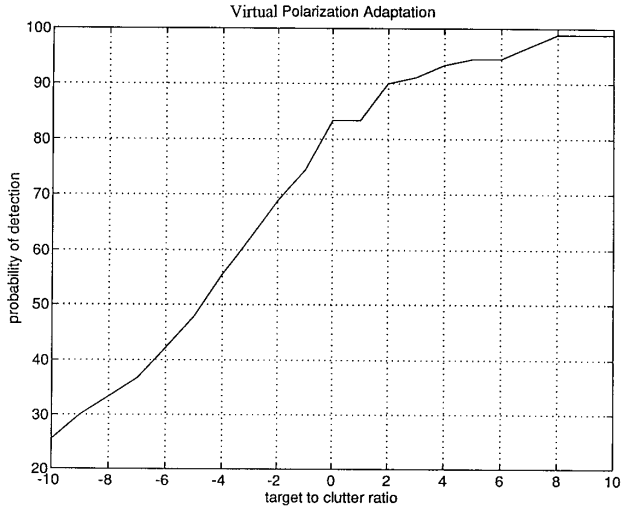

Figure 17. Result of Poelman's VPA procedure.

The one-dimensional K-law assumption achieves better results than Gaussian law modelling for almost any type of clutter and should be used more systematically. However, the derivation of the α parameter is not yet optimal in the case of a polarimetric detector. For the AR modelling scheme, results have been shown in the form of a visibility factor, which is the minimal signal-to-clutter ratio required to get a probability of detection with a fixed probability of false alarm. Using a two-channel polarimetric signal Sinclair vector, instead of a one-channel complex signal AR modelling approach, improves the detection by a factor of 2 dB. More generally, we have shown that polarimetry always improves detector performance, and the improvement can reach up to 7 dB.

Merging the two main detection approaches into one, in order to use their respective advantages makes up the next step of this study. Also, deriving the Neyman-Pearson test for other assumptions (Multi-dimensional complex Weibull or Gamma distributions, etc.) may seem very interesting, although difficult.

As this feasibility approach provides good and promising results, all of these different polarimetric procedures have to be applied now and to be retested against many more meaningful measured data sets, in order to obtain realistic probabilities of false alarm.

ACKNOWLEDGEMENTS

This project was supported by the D.G.A.- D.R.E.T under financial contract No. SJ/RCM no 686.1.

The authors are gratefully indebted to Professor W-M. Boerner, from the Communications Sensing and Navigation Laboratory, University of Illinois at Chicago, whose inspiring influence and initiatives of expanding on the first version of this paper, and his advice and support were particularly highly appreciated.

REFERENCES

1. Aluffi Pentini, F., A. Farina, and F. Zirilli, "Radar detection of targets located in a coherent K distributed clutter background," *Proceedings IEE, Radar and Signal Processing,* Vol. 139, No. 3, June 1992.
2. Belhadj, Z., "Modélisation du fouillis et analyse du Speckle," Ph.D. thesis, IRESTE, Université de Nantes, September 1995.
3. Boerner, W. M., "Polarimetry in wideband interferometric sensing and imaging of terrestrial and planetary environments," invited paper, *Third International Workshop on Radar Polarimetry* (dedicated to Professor W. M. Boerner), March 1995, IRESTE, Nantes, France. ISBN 2-909805-04-2.
4. Boerner, W. M, M. Walther, and A. Segal, "The concept of the polarimetric matched signal and image filters : application to radar target versus clutter optimal discrimination in microwave imaging and sensing," *Int'l Journal on Advances in Remote Sensing (IJARS)*, (EARSEL). Boulogne-Billancourt, France, Vol. 2, No. 1-1, 219–252, January 1993. ISBN 0-7923-1496-4.
5. Boerner, W. M., C. L. Liu, and X. Zhang, "Comparison of the optimization procedures for the 2x2 Sinclair and the 4x4 Mueller matrices in coherent polarimetry and its application to radar target versus background clutter discrimination in microwave sensing and imaging," *Int'l Journal on Advances in Remote Sensing (IJARS)*, (EARSEL). Boulogne-Billancourt, France, Vol. 2, No. 1-1, 55–82, January 1993. ISBN 0-7923-1496-4.

6. Boerner, W. M., et al., Eds., "Direct and inverse methods in radar polarimetry," *Proc. NATO Advanced Research Workshop on DIMRP,* Bad Windsheim, FR Germany, Sept. 18–24, 1985, NATO-ASI Series, Series C: Math and phys Sci., Vol. C-350, Dordrecht, Holland : Kluwer Academic Publ. Co., (1,938 pgs.) February 1992.
7. Boerner, W. M., W. L. Yan, A. Q. Xi, and Y. Yamaguchi, "On the principles of radar polarimetry (invited review) : the target characteristic polarization state theory of Kennaugh, Huynen's polarization fork concept and its extension to the partially polarized case," *IEEE Proceedings, Special Issue on Electromagnetic Theory,* Vol. 79, No. 10, 1538–1550, October 1991.
8. Cloude, S. R., "Polarimetry : the characterization of polarization effects in electromagnetic scattering," Birmingham, UK : University of Birmingham, dissertation (1986).
9. Cloude, S. R., "An entropy based classification scheme for polarimetric SAR data," *IGARSS'95*, 2000–2002, Firenze, Italy.
10. Cloude, S. R., and E. Pottier, "Concept of polarization entropy in optical scattering," *SPIE, Optical Engineering, Special Issue on 'Polarization analysis and measurement'*, Vol. 34, No. 6, 1599–1610, 1995.
11. Cloude, S. R, and Y. Q. Yin, "Numerical eigen analysis of coherence matrix for a layer of random non-spherical scatterers," *IEEE Trans. GRS*, Vol. 32, No. 11, 1179–1185, November 1994.
12. Cloude, S. R, and E. Pottier, "A review of target decomposition theorems in radar polarimetry," *IEEE Trans. GRS*, Vol. 34, No. 3, 498–518, March 1996.
13. Cloude, S. R., and E. Pottier, "An entropy / α parameter based classification scheme for land/sea applications for the interpretation of POL-SAR data takes," *IEEE Trans. GRS*, Vol. 37, No. 1, January 1997 - acc.
14. Goodman, N. R., "Statistical analysis based on a certain multivariate Gaussian distribution (An introduction)," *Ann. Math. Statist.*, 152–176, 1963.
15. Huynen, J. R., "Phenomenogical theory of radar targets," Ph.D. dissertation, DRUKKERIJ BRONDER-OFFSET N.V., Rotterdam, 1970.
16. Huynen, J. R., "Polarimétrie des cibles radar," *First International Workshop on Radar Polarimetry,* IRESTE, Nantes, 21–23 March 1990.

17. Huynen, J. R., "Polarization discrimination theory with applications to target classification and identification," *Second Workshop on Polarimetry Radar Technology.* US-ARMY Missile command, Redstone Arsenal, AL, 1983.
18. Huynen, J. R., "The Stokes matrix parameters and their interpretation in terms of physical target properties," *First International Workshop on Radar Polarimetry,* IRESTE, Nantes, 21–23 March 1990.
19. Huynen, J. R., "Extraction of target significant parameters from polarimetric data," *Report No. 103.* P.Q. Research, Los Altos Hills, California. July 1988.
20. Huynen, J. R., "Towards a theory of perception for radar targets," *Inverse Methods in Electromagnetic Imaging,* Borner W. M. Ed., 797–822, D. Reidel Publishing co Dordrecht, The Netherlands, 1985.
21. Kay, S. M., *Modern Spectral Estimation Theory and Application*, Prenctice Hall signal processing series.
22. Kennaugh, E. M., "Polarization properties of radar reflection," Antenna Laboratory. The Ohio State University Research Foundation. Columbus, Report 389-12 (AD 2494), March 1952.
23. Lee, J. S., M. R. Grunes, and R. Kwok, "Classification of multilook polarimetric SAR imagery based on complex Wishart distribution," *Int'l Journal Remote Sensing*, Vol. 15, No. 11, 2299–2311, 1994.
24. Lee, J. S., M. R. Grunes, K. W. Hoppel, S. A. Mango, and A. R. Miller, "Intensity and phase statistics of multi-look and interferometric SAR imagery," *IEEE Trans. GRS,* Vol. 32, No. 5, 1017–1028, September 1994.
25. Morin, X., E. Pottier, J. Saillard, C. Pasdeloup, and C. Delhote, "Polarimetric detection of slowly moving targets embedded in ground clutter," *Third International Workshop on Radar Polarimetry,* IRESTE, Nantes, March 1995. ISBN 2-909805-04-2.
26. Mott, H., and W. M. Boerner, Eds., *Radar Polarimetry*, SPIE'92 International Symposium, San Diego, CA, 1992 July 20–25, Radar Polarimetry Conference, SPIE, Vol. 1748, 1993.
27. Mott, H., *Antennas for Radar Communications - A Polarimetric Approach*, John Wiley and Sons Ed., New York, 1992.
28. Mott, H., and W. M. Boerner, "Closed form derivation of the OPCE coefficients for the coherence [J], the Sinclair [S], the Kennaugh [K], and the non- unique covariance [Σ] matrices and its comparison proceedings," *Fourth USA-MI-COM Workshop on MMW-THz-IR-OPT polarimetry,* Sparkman Center Auditorium, Redstone Arsenal, AL, 5-7 December 1995.

29. Novak, L. M., M. B. Setchtin, and M. C. Burl, "Algorithms for optimal processing of polarimetric radar data," *Polarimetric Technology Handbook,* GACIAC HB 92–01, 139–206, Chicago, January 1992.
30. Novak L. M., and M. C. Burl, "Optimal Speckle reduction in polarimetric SAR imagery," *IEEE Trans. AES,* Vol. 26, No. 2, March 1990.
31. Novak, L. M., M. C. Burl, and W. W. Irving, "Optimal polarimetric processing for enhanced target detection," *IEEE Trans. AES*, Vol. 29, No. 1, January 1993.
32. Pasdeloup, C., X. Morin, E. Pottier, J. Saillard, and C. Delhote, "Etude et application de procédures polarimétriques. Détection de cibles terrestres de faible S.E.R," 15^{ieme} colloque GRETSI, Juan Les Pins, September 1995.
33. Poelman, A. J., "Virtual polarization adaptation. A method of increasing the detection capability of a radar system through polarization vector processing," *Proceedings IEE*, Pt 1981, Vol. 128, No. 5, 261–270.
34. Poelman, A. J., "Polarization vector translation in radar system," *Proceedings IEE*, Pt 1983, Vol. 130, No. 2, 161–165.
35. Poelman, A. J., "Non-linear polarization vector translation in radar systems : a promising concept for real time polarization vector signal processing via a single notch polarization suppression filter," *Proceedings IEE*, Pt 1984, No. 131, 451–465.
36. Poelman, A. J., and J. R. F. Guy, "Multinotch logic-product polarization suppression filters. A typical design example and its performance in a rain clutter environment," *Proceedings IEE,* Pt 1984, Vol. 131, No. 4.
37. Poelman, A. J., and K. J. Hilgers, *The Effectiveness of Multi-Notch Logic Product Polarization Filters in Radar for Countering Rain Clutter*, Kluwer Academic Publishers, 1992.
38. Pottier, E., and J. Saillard, "Fondements mathématiques de la polarimétrie et son application au domaine du radar," *Annales des télécommunications,* 47, No. 7–8, 314–336, 1992.
39. Sekine, M., and Y. Mao, *Weibull Radar Clutter,* London, UK, Peter Peregrinus Ltd., IEE Publ., 1990.
40. Tur, M., K. C. Chin, and J. W. Goodman, "When is speckle noise multiplicative?" *Applied Optics,* Vol. 21, No. 7, 1157–1159, April 1982.
41. Yueh, S. H., J. A. Kong, J. K. Jao, R. T. Shin, H. A. Zebker, T. Le Toan, and H. Öttl, "K-distribution and polarimetric terrain radar clutter," *Progress In Electromagnetics Research,* PIER 3, edited by J. A. Kong, Elsevier Science Publishing Co., Inc, 1990.